International Conference on Space Optics—ICSO 2022

Dubrovnik, Croatia

3–7 October 2022

Edited by Kyriaki Minoglou, Nikos Karafolas, and Bruno Cugny,

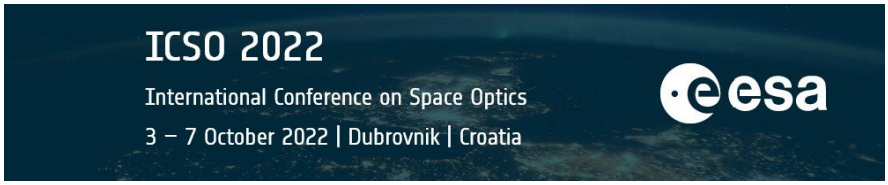

Multilayer coating analysis for heat rejection on the Slit Assembly of Solar-C EUVST

International Conference on Space Optics — ICSO 2022, edited by Kyriaki Minoglou, Nikos Karafolas, Bruno Cugny, Proc. of SPIE Vol. 12777, 127775J · © 2023 ESA and CNES · 0277-786X · doi: 10.1117/12.2691028

Multilayer coating analysis for heat rejection on the Slit Assembly of Solar-C EUVST

Zeni Gabriele [3,1]* , Corso Alain Jody [1] , Cocola Lorenzo [1] , Giovine Ennio [2] , Mattioli Francesco [2] , Naletto Giampiero [1,3,4] , Andretta Vincenzo [5] , Poletto Luca [1]

[1] CNR-Institute for Photonics and Nanotechnologies, Via Trasea 7, 35131, Padova, Italy
[2] CNR-Institute for Photonics and Nanotechnologies, via Cineto Romano 42, 00156, Roma, Italy
[3] CISAS - Centre of Studies and Activities for Space "Giuseppe Colombo", Via Venezia 15, 35131, Padova, Italy
[4] University of Padua, Dept Phys & Astron, Via F Marzolo 8, I-35131, Padova, Italy
[5] INAF Astronomical Observatory Capodimonte, Salita Moiariello 16, 80131, Napoli, Italy

ABSTRACT

Solar-C EUVST is a collaboration among Japan, US and several European countries. The goal of EUVST is to study the solar atmosphere in the extreme UV, using a spectrometer and a Slit-Jaw Imager as the main instrumentation. One of the key components of both instruments is the Slit Assembly, which is provided by the Italian Space Agency. In the baseline design, the Slit Assembly consists of a thin silicon wafer with several slits placed on the telescope focal plane. Since the slit substrate is illuminated by the focused broadband solar spectrum, the resulting thermal load may potentially be a problem. In order to maximize reflection and minimize heat absorption, and also to have high reflectance in the operating wavelength of the Slit-Jaw Imager, a specifically designed optical coating is required for the slit substrate. Due to the narrow width of the scientific slits, it is also important for the optical coating to have a thickness much smaller than the slit width, in order to avoid problem of shrinkages or partial obstruction of the slits during the deposition process. Considering these constraints, different typologies of optical coatings were analyzed in this theoretical study. We analyzed several configurations of metal and protective coatings, using a genetic algorithm to optimize the number and thickness of the layers. Among the analyzed configurations, two multilayers exhibit the best performance: a standard multilayer based on six layers of Al_2O_3 and SiO_2 and a more exotic multilayer coating based on seven layers of ZrO_2 and SiO_2.

Keywords: multilayers, slit, reflectance, absorption, genetic algorithms

1. INTRODUCTION

Solar-C EUVST (EUV High-throughput Spectroscopic Telescope) is the fourth mission selected by the Japan Aerospace Exploration Agency (JAXA) after the 2017 call for Medium-sized Focused Missions [1]. Scheduled to be launched in 2027, Solar-C EUVST is the successor of the very successful Solar-A (Yohkoh) and Solar-B (Hinode). The mission is a collaboration among Japan, US and several European countries.

*gabriele.zeni.1@phd.unipd.it

Solar-C EUVST mission is designed to understand how mass and energy are transferred throughout the entire solar atmosphere. Two are the primary science objectives [1]:

- To understand how fundamental processes lead to the formation of the solar atmosphere
- To understand how the solar atmosphere becomes unstable, releasing the energy that drives solar flares and eruptions.

In order to achieve the two science objectives, the mission has to: observe all temperature regimes of the solar atmosphere; resolve elemental structures of the solar atmosphere and track their changes; obtain spectroscopic information on dynamics of elementary processes taking place into the solar atmosphere [1].

The most suitable wavelength bands to be investigated have been identified into the vacuum ultraviolet (VUV), comprising both the extreme ultraviolet (EUV – from 10 to 120 nm) and the far ultraviolet (FUV – from 120 to 200 nm). Solar-C EUVST will actually observe specifically four narrow bands: 17.0-21.5 nm (short wavelength sensor, SW), 69.0-85.0 nm (long wavelength sensor, LW1), 92.5-108.5 nm (LW2), 111.5-127.5 nm (LW3) [1]. The US instrument, the Slit-Jaw Imager, will observe a narrow wavelength band, from 279.6 nm to 285.2 nm (corresponding to the line of Mg II and Ca II [2]).

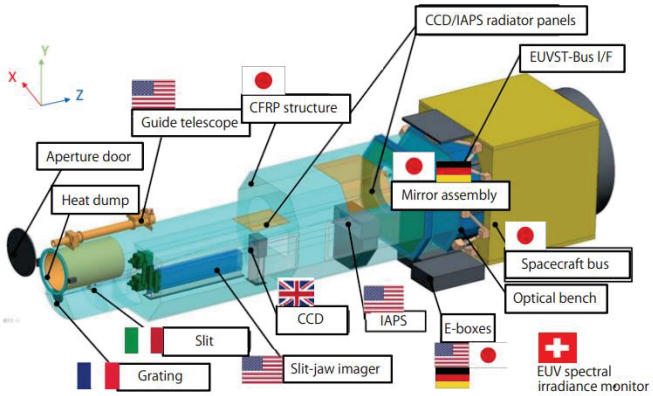

Figure 1. Solar-C EUVST structure [2].

The main onboard instrument of Solar-C are the spectrograph and the Slit-Jaw Imager. A key component of both instruments is the Slit Assembly, provided by the Italian Space Agency (ASI). In the baseline design, the Slit Assembly consists of a thin silicon wafer with several slits placed on the telescope focal plane. The slits select the spatial portion of the beam transmitted to the spectrometer while, at the same time, the area around the slits back-reflects most of the light onto the Slit-Jaw Imager channel where the Sun disk is re-imaged. Since the slit substrate is therefore illuminated by the focused broadband solar spectrum, the resulting thermal load may potentially constitute a problem. To avoid any thermal issue, a proper optical coating is required, maximizing reflection and minimizing heat absorption. In addition of having high reflectivity in the visible and near-IR portions of the Solar spectrum, where most of the thermal load is concentrated, the optical coating should also have high reflectance in the narrow bandpass centered at 280 nm, where the Slit-Jaw Imager is operative.

The Slit Assembly (SA) has 4 scientific slits and a calibration pinhole realized on a silicon substrate. The baseline design includes 0.2, 0.4, 0.8, and 1.6 arcsec science slits, each 300 arcsec in length. The width of the narrowest slit is 3.0 µm whereas the calibration pinhole has a diameter of 1.5 µm. Both apertures will be manufactured on the substrate before the deposition of the coating. We have to take in account the smallest slit width in the design of the coating, in order to avoid shrinkages or partial obstructions caused by the growth of the coating during the deposition process. Although no studies have been yet done in the measuring of the magnitude of such effects, it is reasonable to assume that a thicker coating layer will have a much higher impact on the obstruction of the aperture than a thinner one. Given the width of the

narrowest slit, a reasonable value for the maximum coating thickness can be close to 0.6 μm, in order to avoid any partial obstruction of the slit.

2. METHODOLOGY

Considering the characteristics of the Slit Assembly described in the previous section, the main requirements for the Slit Assembly optical coating can be resumed as:

- Reflectance: the substrate of the SA shall have high reflectivity in the bandpass centered at 280 nm and shall reflect most of the incident thermal load
- Thickness: the coating shall not exceed a thickness of 600 nm

These two requirements will lead the analysis of the proposed optical coating. The analysis can be roughly divided into two subsequent phases. In the first phase, we analyze the metallic materials typically used to produce high reflectivity optical devices. Then, in the second phase we analyze different types of protective optical coating, using a genetic algorithm to optimize both the thickness and the optical performance of the coating.

2.1 Metal selection

The wide spectral range in which the coating must guarantee high reflectivity suggests the use of a coating based on a metal layer covered by one or more protective dielectric layers. Three are the typical metals used as reflective layer for the bandpass from the near UV to the FIR: silver, gold and aluminum.
Silver, Ag, although having a high reflectance in the visible and infrared bands, is extremely reactive and prone to surface oxidation/passivation. Moreover, silver shows low UV reflectance due to the absorption edge at 310 nm; in the bandpass centered at 280 nm the reflectance is always below 0.25 [3].
Gold, Au, has no chemical instabilities. Gold is extremely stable on the long term and it could be used without any protective layer, being prone only to mechanical damages. However, gold has low reflectance for wavelengths shorter than 550 nm, resulting in poor reflectance performance in the visible and UV band. In particular, gold reflectivity is 0.37 at 280 nm [4].
Aluminum, Al, has the best behavior, with a high reflectance in the whole spectrum of interest. Its absorption edge is placed well below the 150 nm, so the reflectance in the bandpass centered at 280 nm is extremely high (around 0.9) as well in the visible (>0.9) and IR (>0.95). However, aluminum is reactive and prone to oxidation, so it has to be protected with a dielectric capping-layer [4],[5].
Considering the requirements previously described, we can observe that silver and gold cannot be considered suitable for this specific application, especially since both of them show low UV reflectance and particularly in the wavelength bandpass centered at 280 nm. Therefore silver and gold are not considered valid option to produce an optical coating with the requested characteristics. Aluminum is the metal layer that we consider in the proposed optical coatings.

2.2 Protective layer material selection

Once the metal layer has been chosen, we analyze several different types of dielectric materials which could be used to create one or more protective layers over the metallic layer. We considered six different oxides:

- Silicon dioxide (silica) SiO_2
- Magnesium fluoride MgF_2
- Aluminum oxide (alumina) Al_2O_3
- Titanium dioxide TiO_2
- Zirconium oxide ZrO_2

The first two types of materials, SiO_2 and MgF_2, are commonly used in mirror coating applications. For these two materials we analyze also a single layer protective coating, in order to obtain a baseline and simple solution to be compared to other more complex structures.

We considered the other four materials in the definition of a multilayer structure, in combination with layers of SiO_2 due to its greater stability than MgF_2. The multilayer structures (e.g. number of layers, thickness) has been calculated using a suitable algorithm, as described in the following section.

2.3 Thickness and multilayer structure optimization

The analysis of the proposed single layer and multilayer protective coating has been performed considering the foreseen solar input at the Slit Assembly and then optimizing the structure with respect to the absorbed heat, since the thermal load seems to be the most critical issue for the slit substrate.

The solar input at the slit assembly level is dependent on the characteristics of the primary mirror of EUVST, which focuses the solar radiation on the slit. Multiple different primary mirror coatings have been proposed, and we have considered two different scenarios: a primary mirror with the baseline Mo/Si multilayer coating (P3157), and a primary mirror with a Mo/Al multilayer coating which has a significantly higher reflectivity (N7422). Coating P3157, being the baseline solution, allows a thermal analysis considering rather standard conditions, while coating N7422 allows the analysis at the highest power incident on the slit assembly. The solar input data on slit for the two cases have been collected from [6] and they are summarized in Fig. 2. During the optimization, we have considered the spectrum band between 250 and 1700 nm, that is the band where almost 90% of the total solar energy is concentrated; in this way, the optimization is focused on the most critical portion of the incident spectrum.

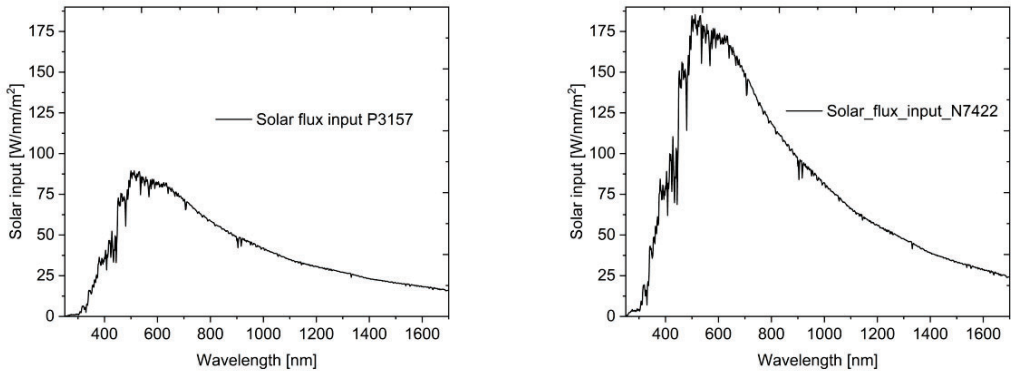

Figure 2. Solar flux input at the Slit Assembly. On the left, for P3157 primary mirror coating; on the right, for N7422 primary mirror coating [6].

The analysis to calculate the thickness of the coating layers has been performed using a genetic algorithm; then the comparison between the different structures has been performed considering the heat absorbed by the analyzed structure. The genetic algorithm, similar to those described in [7], randomly creates a set of initial structures (the first group of "parents") of the optical coating and then the algorithm modifies each individual using processes that are mimicking the natural evolution of a biological being. In particular, we impose an initial population of some tens of randomly generated individuals. Then, we randomly choose two of them to perform a crossover in which a portion of the first parent is combined with a portion of the second parent and vice versa, in order to create two new individuals with the same dimension of the parents but a complete new structure (the same event happens in the genetic crossover). We take these individuals and we perform a mutation of their characteristics, finding finally the new generation. At each step of the process, an evaluation of the individual fitness is performed by comparing the calculated absorbed heat with the best value ever found. So, the calculated absorbed heat works as a "cost function" at each passage of the algorithm, allowing to discard the individuals that are not suitable for our purposes. In order to restrain the calculation time, a maximum number of generations has been imposed, setting it at 2500 with a population of 50 individuals. We have also integrate some boundary conditions considering the maximum thickness value of each single layer, in order to satisfy the

maximum thickness constraint, but especially the minimum thickness value, set at 10 nm due to the typical deposition precision of the standard facility used to produce such types of optical coating.

Once the best stack sequence is found, another optimization algorithm is used to analyze the possible impact of a non-perfect deposition of the layers (i.e., an error in the thickness of the layer during the deposition process). This analysis is crucial to understand if a deviation from the theoretical model can produce a significant variation of the coating performance. A gaussian distribution for the thickness random error is imposed with a sigma of 0.5 nm, according to the errors obtained in standard deposition facilities. This random error is added to each layer and the algorithm calculates the amount of absorbed heat, repeating the process for a thousand of cycles.

3. DATA

The base spectral interval where the coating optimization is performed is the wavelength bandpass 250-1700 nm, where 90% of the solar flux input is concentrated. This is the wavelength region where optical constants are available from the literature for all the proposed materials.
To have a reference in terms of ideal optimal performance, we calculated the absorbed heat for the bare aluminum. In fact, this value can be settled as the theoretical limit with the best performance in terms of reflectivity and corresponding absorbed heat.

Table 1. Baseline theoretical layer and minimum absorbed heat

Baseline bare aluminum coating	
Solar flux input 250-1700 nm	
P3157	2.32 W
N7422	4.57 W
Absorbed heat for bare aluminum	
P3157	0.11 W
N7422	0.36 W

For all the cases, we assumed that a 90-nm thick aluminum layer is deposited on the slit silicon substrate with a 10 nm adhesion layer of chromium; then, on top of the aluminum, the protective layer is deposited.

4. RESULTS

We have considered two main typologies of coatings: 1) *single-layer protected Al,* in which only one layer is deposited on the aluminum, and 2) *multilayer protected Al,* in which a stack of several layers of different materials is deposited on the aluminum.

4.1 Single-layer protected Al coating

Two typical materials for protecting aluminum have been considered: SiO_2 and MgF_2. Both materials are commonly used in mirror coating applications; they are transparent for the spectrum portion of interest, stable and the deposition procedure is well known [8],[9].
Using the optimization algorithm, the results of the optimization of the two types of single layer protected Al coatings are shown in the following table.

Table 2. Data for single-layer protected aluminum coating considering P3157 primary mirror coating

P3157 primary mirror coating				
Label	Structure	Total thickness	Absorbed heat (250-1700 nm)	Reflectivity at 280 nm
SiO_2_single_layer_P3157	SiO_2 (254 nm) Al (90 nm) Cr (10 nm)	354 nm	0.14 W	0.92
MgF_2_single_layer_P3157	MgF_2 (253 nm) Al (90 nm) Cr (10 nm)	353 nm	0.15 W	0.85

Table 3. Data for single-layer protected aluminum coating considering N7422 primary mirror coating

N7422 primary mirror coating				
Label	Structure	Total thickness	Absorbed heat (250-1700 nm)	Reflectivity at 280 nm
SiO_2_single_layer_N7422	SiO_2 (257 nm) Al (90 nm) Cr (10 nm)	357 nm	0.47 W	0.93
MgF_2_single_layer_N7422	MgF_2 (263 nm) Al (90 nm) Cr (10 nm)	363 nm	0.46 W	0.90

The single-layer protected Al coatings have relatively worse performance with respect to the bare Al, since the absorbed heat increases by roughly 30%. However, this type of coating is a simple and robust solution, since it gives high reflectance in the bandpass centered at 280 nm and it has a simple deposition process. SiO_2 has slightly better performance than MgF_2 in terms of higher reflectivity at 280 nm and lower absorbed heat.

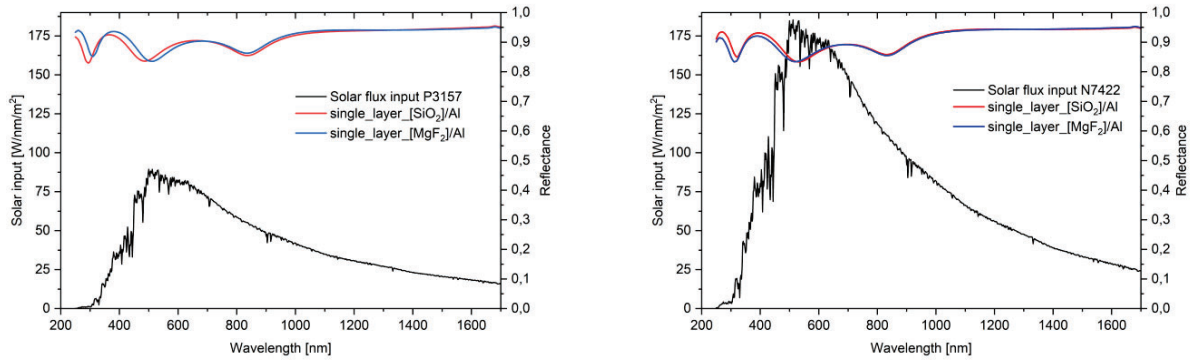

Figure 2. Reflectance of the two single-layer protected Al coatings with P3157 solar input (left) and N7422 solar input (right) [8], [9].

4.2 Multilayer protected al coating

The analysis of the multilayer type of structures is based on the idea of "boosting" the aluminum layer reflection. The coating will be a fully dielectric multilayer in order to improve as much as possible the aluminum reflection to enhance

the heat rejection. Usually, multilayer coatings have tens of different layers, in order reach the maximum efficiency. However, one of the main requirements of the Slit Assembly is on the upper limit of the total thickness of the coating: 600 nm. Considering that each coating would have a 90 nm thick layer of Al and a 10 nm thick layer of Cr, the total amount of thickness for the protective multilayer would be at maximum 500 nm. This fact leads to a multilayer stack in which the number of different layers is small. Also the precision of the deposition process has to be considered, because it depends on the thickness of the deposited layer: the thinner is the layer, the higher is the uncertainty in the deposition process.
Four different types of multilayer stacks have been analyzed; each of these multilayer types considers two different materials, one of these being always SiO_2 for its stable and well-known behavior. The second material is a metallic oxide, chosen from the group of transparent oxide commonly used for mirror coatings. The four types of multilayer stack analyzed are:

- $[MgF_2/SiO_2]/Al$
- $[Al_2O_3/SiO_2]/Al$
- $[TiO_2/SiO_2]/Al$
- $[ZrO_2/SiO_2]/Al$

The resulting multilayer has been analyzed using the IMD software [10].

4.2.1 $[MgF_2/SiO_2]/Al$, 6 layers

The first type of multilayer structure is simply the combination of the two materials used in the single layer baseline coatings. The multilayer has indeed roughly the same absorbed heat of the single layer, therefore it is not considered as a suitable solution since it simply increases the complexity of the coating.

Table 4. Data for the 6-layers $[MgF_2/SiO_2]/Al$ coating, considering P3157 primary mirror coating

P3157 primary mirror coating				
Label	Structure	Total thickness	Absorbed heat (250-1700 nm)	Reflectivity at 280 nm
$[MgF_2/SiO_2]/Al$ 6 layers _ P3157	MgF_2 (22 nm) SiO_2 (71 nm) MgF_2 (23 nm) SiO_2 (70 nm) MgF_2 (46 nm) SiO_2 (20 nm) Al (90 nm) Cr (10 nm)	352 nm	0.14 W	0.86

Table 5. Data for the 6-layers $[MgF_2/SiO_2]/Al$ coating, considering N7422 primary mirror coating

N7422 primary mirror coating				
Label	Structure	Total thickness	Absorbed heat (250-1700 nm)	Reflectivity at 280 nm
$[MgF_2/SiO_2]/Al$ 6 layers _ N7422	MgF_2 (22 nm) SiO_2 (71 nm) MgF_2 (21 nm) SiO_2 (51 nm) MgF_2 (68 nm) SiO_2 (15 nm) Al (90 nm) Cr (10 nm)	316 nm	0.47 W	0.85

[Al_2O_3/SiO_2]/Al, 6 layers

The second type of multilayer has a common metal oxide, alumina Al_2O_3, as second type of material to be combined with SiO_2. Al_2O_3 is a stable well-known material [11]. This multilayer has an absorbed heat respectively of 0.12 W considering P3157 primary mirror coating and 0.39 W considering N7422 primary mirror coating, much closer to bare aluminum than the single layer coating.

Table 6. Data for the 6-layers [Al_2O_3/SiO_2]/Al coating, considering P3157 primary mirror coating

P3157 primary mirror coating				
Label	Structure	Total thickness	Absorbed heat (250-1700 nm)	Reflectivity at 280 nm
[Al_2O_3/SiO_2]/Al, 6 layers	Al_2O_3 (113 nm) SiO_2 (105 nm) Al_2O_3 (34 nm) SiO_2 (24 nm) Al_2O_3 (99 nm) SiO_2 (87 nm) Al (90 nm) Cr (10 nm)	562 nm	0.12 W	0.81

Table 7. Data for the 6-layers [Al_2O_3/SiO_2]/Al coating, considering N7422 primary mirror coating

N7422 primary mirror coating				
Label	Structure	Total thickness	Absorbed heat (250-1700 nm)	Reflectivity at 280 nm
[Al_2O_3/SiO_2]/Al, 6 layers	Al_2O_3 (94 nm) SiO_2 (34 nm) Al_2O_3 (34 nm) SiO_2 (81 nm) Al_2O_3 (28 nm) SiO_2 (35 nm) Al (90 nm) Cr (10 nm)	406 nm	0.39 W	0.90

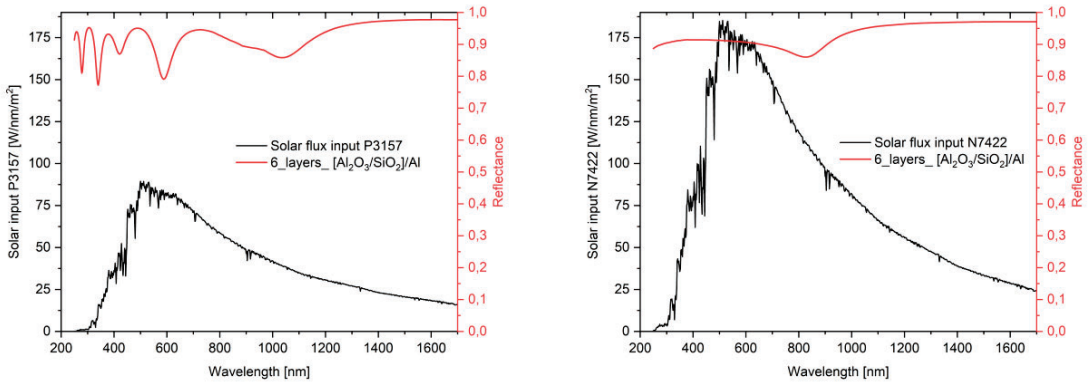

Figure 3. Reflectance of the 6-layers [Al_2O_3/SiO_2]/Al coatings with P3157 solar input (left) and N7422 solar input (right) [11]

[TiO_2/SiO_2]/Al, 6 layers

The third type of analyzed multilayer uses a classical coating material, the titanium dioxide TiO_2. TiO_2/SiO_2 multilayer is widely used in mirror coating manufacturing because it shows extremely good characteristics: very stable behavior with high durability and a low mechanical stress [12]. Also, the TiO_2 has one of the highest index of refraction in the visible band, so it is extremely useful to generate low reflecting film in combination with other materials like SiO_2. Indeed, the multilayer [TiO_2/SiO_2]/Al has a calculated absorbed heat of 0.16 W and 0.36 W considering the two types of primary mirror coating, close to that of the bare aluminum. However, a drop of the reflectance curve occurs in the UV region because of the absorption edge of the TiO_2 at 350 nm. This gives a low reflectance at 280 nm, that is considered as a major limitation for such a coating.

Table 8. Data for the 6-layers [TiO_2/SiO_2]/Al coating, considering P3157 primary mirror coating

P3157 primary mirror coating				
Label	Structure	Total thickness	Absorbed heat (250-1700 nm)	Reflectivity at 280 nm
[TiO_2/SiO_2]/Al, 6 layers	TiO_2 (23 nm) SiO_2 (67 nm) TiO_2 (20 nm) SiO_2 (81 nm) TiO_2 (97 nm) SiO_2 (88 nm) Al (90 nm) Cr (10 nm)	476 nm	0.16 W	0.56

Table 9. Data for the 6-layers [TiO_2/SiO_2]/Al coating, considering N7422 primary mirror coating

N7422 primary mirror coating				
Label	Structure	Total thickness	Absorbed heat (250-1700 nm)	Reflectivity at 280 nm
[TiO_2/SiO_2]/Al, 6 layers	TiO_2 (86 nm) SiO_2 (100 nm) TiO_2 (74 nm) SiO_2 (22 nm) TiO_2 (64 nm) SiO_2 (22 nm) Al (90 nm) Cr (10 nm)	468 nm	0.36 W	0.35

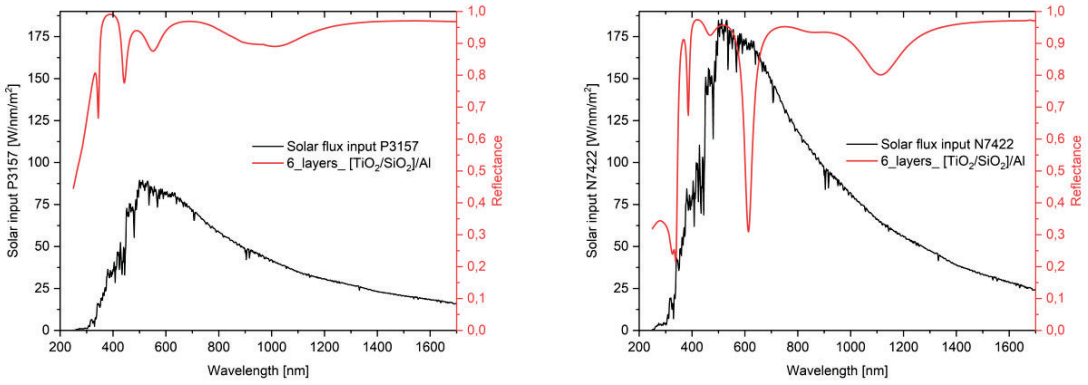

Figure 4. Reflectance of the 6-layers [TiO_2/SiO_2]/Al coatings with P3157 solar input (left) and N7422 solar input (right) [12]

[ZrO_2/SiO_2]/Al, 7 layers

The fourth type of multilayer analyzed uses another material often used in mirror coatings application, the zirconia or zirconium dioxide ZrO_2; the optical characteristics of this material has been extrapolated with Sellmeier dispersion formula from previous transmittance measurements. In combination with SiO_2, it is used to create multilayer coatings with high durability and low mechanical stress. The multilayer stack consists of 7 layers, and not 6 like the others multilayer coatings here described, because the long exposition to UV can damage an exposed ZrO_2 layer. In order to protect the coating in a long-term mission, the layer facing directly the space is assumed to be SiO_2, more durable and stable. [ZrO_2/SiO_2]/Al multilayer has a calculated absorbed heat of 0.12 W and 0.36 W, with a performance very close to bare aluminum. The zirconium dioxide has a reflection drop in the UV centered at 230 nm, therefore the reflectance of the multilayer in the region around 280 nm is higher than those of the titanium dioxide multilayer.

Table 10. Data for the 7-layers [ZrO_2/SiO_2]/Al coating, considering P3157 primary mirror coating

P3157 primary mirror coating				
Label	Structure	Total thickness	Absorbed heat (250-1700 nm)	Reflectivity at 280 nm
[ZrO_2/SiO_2]/Al, 7 layers	SiO_2 (22 nm) ZrO_2 (75 nm) SiO_2 (83 nm) ZrO_2 (20 nm) SiO_2 (43 nm) ZrO_2 (90 nm) SiO_2 (81 nm) Al (90 nm) Cr (10 nm)	514 nm	0.12 W	0.80

Table 11. Data for the 7-layers [ZrO_2/SiO_2]/Al coating, considering N7422 primary mirror coating

N7422 primary mirror coating				
Label	Structure	Total thickness	Absorbed heat (250-1700 nm)	Reflectivity at 280 nm
[ZrO_2/SiO_2]/Al, 7 layers	SiO_2 (40 nm) ZrO_2 (74 nm) SiO_2 (82 nm) ZrO_2 (25 nm) SiO_2 (32 nm) ZrO_2 (90 nm) SiO_2 (80 nm) Al (90 nm) Cr (10 nm)	523 nm	0.36 W	0.72

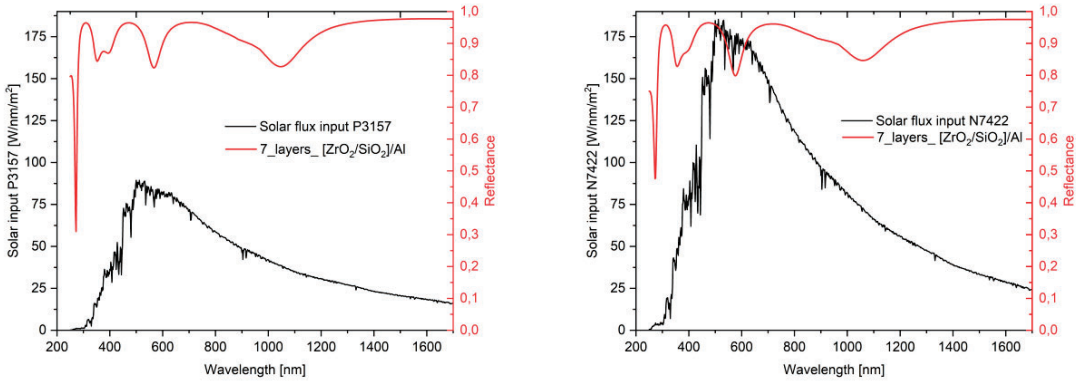

Figure 5. Reflectance of the 7-layers [ZrO_2/SiO_2]/Al coatings with P3157 solar input (left) and N7422 solar input (right)

4.3 Coating thickness random error

The thickness error analysis has been performed adding a random (gaussian) error with a sigma of 0.5 nm at the single layer of the single layer protected Al coating or at each layer of the multilayer protected Al coating. An optimization algorithm has been created to analyze the absorbed heat, then the mean value of absorbed heat and the standard deviation have been calculated. The analysis shows that the deposition error expected in a standard deposition facility has a negligible impact on the absorbed heat, with an extremely low standard deviation. It can be concluded that, once the stack has been optimized, the effect of a random error in the thickness of the layers is negligible.

5. CONCLUSIONS

5.1 Reflected and absorbed heat

The analysis shows that the $[MgF_2/SiO_2]$/Al multilayer has no advantages with respect to the single layer coatings and simply increases the complexity of the optical coating. The $[TiO_2/SiO_2]$/Al multilayer, on the other hand, has performance slightly worse than those of the $[ZrO_2/SiO_2]$/Al multilayer, especially from the point of view of the reflectivity in the bandpass centered at 280 nm. Due to these reasons, both $[MgF_2/SiO_2]$/Al and $[TiO_2/SiO_2]$/Al multilayers are not considered as suitable . In the following analysis we will concentrate on the other types of proposed multilayer coatings.
The following tables summarize the reflected and absorbed heat.

Table 12. Reflected and absorbed heat for all the proposed configurations, considering P3157 primary mirror coating

P3157 Primary Mirror Coating		
Slit coating	Absorbed Heat (250-1700 nm)	Reflected Heat (250-1700 nm)
Bare Al (reference)	0.11 W	2.21 W
Al + single layer [SiO_2 or MgF_2]	0.15 W	2.18 W
$[Al_2O_3/SiO_2]$/Al, 6 layers	0.12 W	2.20 W
$[ZrO_2/SiO_2]$/Al, 7 layers	0.12 W	2.20 W

Table 13. Reflected and absorbed heat for all the proposed configurations, considering N7422 primary mirror coating

N7422 Primary Mirror Coating		
Slit coating	Absorbed Heat (250-1700 nm)	Reflected Heat (250-1700 nm)
Bare Al (reference)	0.36 W	4.21 W
Al + single layer [SiO_2 or MgF_2]	0.47 W	4.10 W
$[Al_2O_3/SiO_2]$/Al, 6 layers	0.39 W	4.18 W
$[ZrO_2/SiO_2]$/Al, 7 layers	0.36 W	4.21 W

Considering both the absorbed heat and the reflectivity at 280 nm, two multilayer coatings could be considered as the most interesting types of slit substrate coatings: the 6 layers coating $[Al_2O_3/SiO_2]$/Al and the 7 layers coating $[ZrO_2/SiO_2]$/Al. The former has a higher reflectivity in the band centered at 280 nm and it has a relatively known behavior, while the latter has a slightly better heat rejection performance.
Concerning the total heat reflected toward the Slit-Jaw Imager (mainly in the visible and near IR bands), this varies by almost a factor 2 with the coating on the primary mirror, but is almost independent of the coating that is used on the slit assembly.
Further analysis must be performed to address the mechanical behavior and the lifetime of the coating, in order to obtain a complete characterization of the optical coating and to collect the data necessary to choose the best solution for the Slit Assembly of Solar-C EUVST.

REFERENCES

[1] Shimizu et al., "The Solar-C (EUVST) mission: the latest status", Proc. of SPIE vol. 11444 (2020)
[2] NASA EUVST Concept Study Report
[3] Werner W. S. M. et al., "Optical Constants and Inelastic Electron-Scattering Data for 17 Elemental Metals", Journal of Physical and Chemical Reference Data, Vol. 38, No. 4 (2009)
[4] Hagemann H. J. et al., "Optical constants from the far infrared to the x-ray region: Mg, Al, Cu, Ag, Au, Bi, C, and $A1_20_3$", Journal Of The Optical Society Of America, Vol. 65, No. 6 (1975)
[5] McPeak K. M. et al., "Plasmonic Films Can Easily Be Better: Rules and Recipes", ACS Photonics (2015)
[6] Suematsu Y., Solar flux input (personal communication, October 2021)
[7] Goldberg D. E., "Genetic Algorithm in Search, Optimization and Machine Learning", Addison-Wesley Professional (1989)
[8] Gao L. et al., "Exploitation of multiple incidences spectrometric measurements for thin film reverse engineering", Optic Express, Vol. 20, No. 14 (2012)
[9] Rodriguez-DeMarcos L. V. et al., "Self-consistent optical constants of MgF_2, LaF_3 , and CeF_3 films", Optical Material Express, Vol. 7, No. 3 (2017)
[10] Windt D. L., "IMD: Software for modeling the optical properties of multilayer films," Comput. Phys. 12(4), 360–370 (1998), http://www.rxollc.com/idl/index.html.
[11] Querry M. R., "Optical Constants", Univ of Missouri (1985)
[12] Siefke T. et al., "Materials Pushing the Application Limits of Wire Grid Polarizers further into the Deep Ultraviolet Spectral Range", Advance Optical Materials (2016)